PART SCALING AND MECHANICS OF THIN PART SELF-ASSEMBLY IN THE FLUDIC PHASE

Kwang Soon Park[1], Xugang Xiong[1], Rajashree Baskaran[1,2], Karl F Böhringer[1]
[1]Department of Electrical Engineering, University of Washington, Seattle, USA
[2]Components Research, Intel Corporation, USA

ABSTRACT

This paper presents an experimental and theoretical study of previously demonstrated high yield self-assembly processes using surface programmable template and specific surface Faraday waves. Here we focus on the combined effect of substrate tilting angle and part size. For 1×1, 3×3 and 5×5 mm^2 parts of 100 µm thickness, the maximum substrate tilting angles for effective assembly are experimentally determined and the surface tension induced torques are calculated based on a newly developed model.

INTRODUCTION

Fluidic self-assembly (FSA) is a promising alternative to conventional serial pick-and-place assembly. Mechanical serial pick-and-place assembly enables high yield. For small size parts, however, it becomes slow and difficult to control due to undesirable strong stiction forces. Therefore, for assembly of large numbers of small and thin parts, conventional pick-and-place assembly becomes costly and FSA is preferred. Previous FSA systems have used various driving forces such as gravity [1], surface tension [2-4], electrostatic [5], electromagnetic force [6, 7] and often require adhesives, liquid solder, shape matching structures or two different liquids [8]. They, however, have lower yield compared to pick-and-place assembly due to their stochastic nature [9].

The analysis of FSA at an air-water interface indicates that there is a limit on the lateral dimension of the parts that can be assembled when we use a constant substrate tilting angle. Based on this analysis, we develop a new approach that is capable of assembling parts of higher lateral dimensions using parametric changes in substrate tilting angle. We also develop a simulator for the part motion on Faraday waves and observe how the waves can accelerate the part approach.

SYSTEM SETUP

Our system consists of a water container on a linear electromagnetic vertical vibration table (Brüel & Kjær Type 4809), a dip coater (KSV Dip Coater), a substrate and parts floating at an air-water interface (Figure 1). The acceleration uniformity over the vibration table is 0.72 % or +/– 10 mg as measured using a laser vibrometer (Polytec OFV-534 laser unit and OFV-2500 vibrometer controller) when driven at 80 Hz / 1.4 g.

The assembly substrate is fabricated from a 4 inch silicon wafer coated with Cr (10 nm) and Au (100 nm) by electron beam evaporation. The wafer is spin coated with AZ4620 resist followed by photolithography to define the square patterns. The exposed Au and Cr layers are removed subsequently using wet etching. A standard Bosch DRIE (deep reactive ion etch) process is used to etch the exposed silicon sites to approximately 70 µm depth. After photoresist removal, the patterned substrate is cleaned in oxygen plasma and then soaked in a solution of 1 mM dodecanethiol in ethanol overnight. A thiol SAM (self-assembled monolayer) selectively attaches to the gold surface and makes them hydrophobic. The wafer substrate is then diced into several pieces for assembly tests.

Fabrication of thin parts is achieved by standard photolithography, Cr/Au evaporation, wet-etch and dry-etch steps on the front side of the SOI wafer. Dry-etching exposes the buried oxide layer and HF etching releases parts. Then individual parts are stored in ethanol solution.
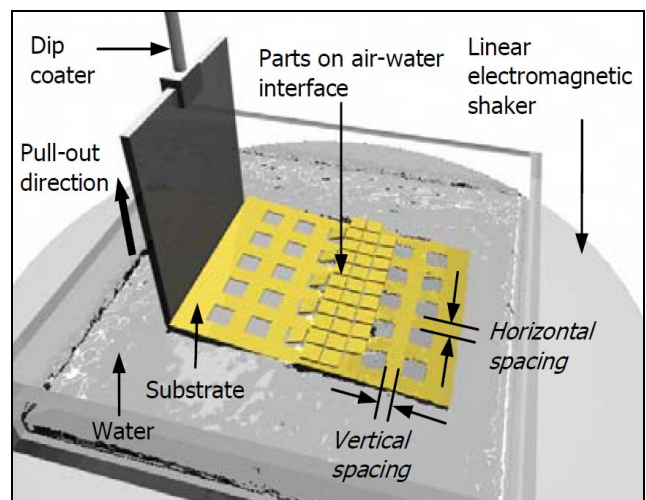
Figure 1. *The experimental setup consists of a water container, linear electromagnetic vibration table, dip coater with affixed substrate and parts floating at the air-water interface.*

The substrate can be tilted at any angle with the water surface and pulled up vertically by a dip coater. This angle is optimized from experimental data and analytical models to be discussed later in this paper. During substrate pull-up, parts approach the substrate due to the meniscus formed by the hydrophobic (SAM-coated Au) / hydrophilic (Si) patterns on the substrate.

The shape of the meniscus changes depending on the substrate tilting angle (Figure 2). The meniscus convexity $\theta*$ is defined by equation (1) where α is the plate tilting angle and θ is the contact angle between substrate and water.

$$\theta^* = \theta + 90° - \alpha \qquad (1)$$

The meniscus becomes flat at α_c, which is the critical condition for parts to approach the substrate. For the substrate tilting angles larger than α_c, parts do not approach the substrate and there is no assembly.

In a FSA system, the parts go through three steps before successful assembly (Figure 3). Parts at the air-water interface approach the substrate and make line contact if the meniscus is smooth enough for parts to approach in step (a). As shown in Figure 4, a steep slope prevents the part approach because the part keeps flat contact with water. A large part needs a large α to approach the substrate. As the substrate is pulled up, the meniscus convexity changes from downward to upward due to surface tension of the water and hydrophilic property of binding site. During transition from (b) to (c) in Figure 3, the part at the substrate-water interface rotates by the angle α, which induces the capillary torque. Thus the capillary torque between parts and binding site plays a decisive role in the assembly process.

Specific surface Faraday waves are also applied at every row to achieve one-to-one part-to-substrate registration (Figure 5(b) and (c)), which enables 100 % yield (Figure 5(d)). Faraday waves also help parts approach to a substrate and are simulated based on [10, 11]. The simulation result in Figure 6 shows that Faraday waves accelerate part approach to the substrate.
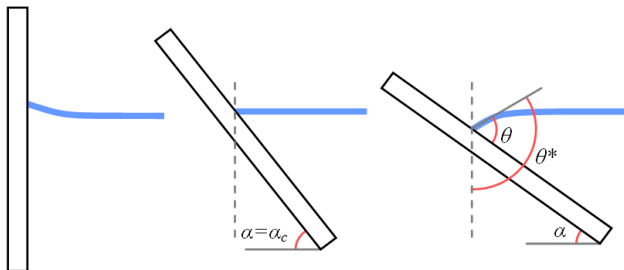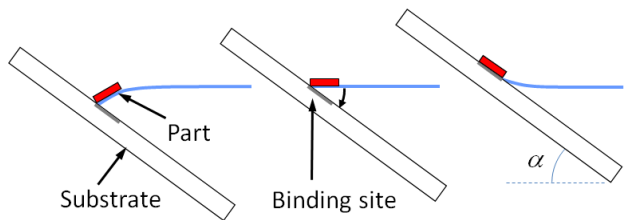

Figure 4. Part $(3000 \times 3000 \times 100\ \mu m^3)$ approaching the substrate. (a) Abrupt change of meniscus slope prevents the part approach. (b) Low convexity helps part approach. Photographs with water colored blue.
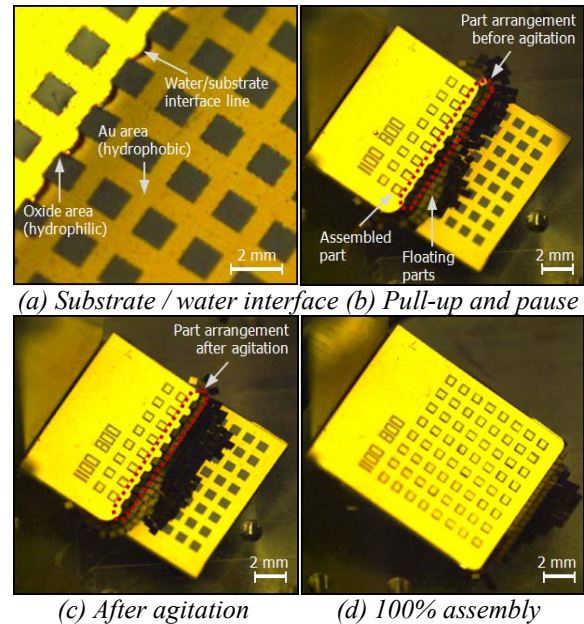
(a) Substrate / water interface (b) Pull-up and pause

(c) After agitation (d) 100% assembly

Figure 5. Parts $(3000 \times 3000 \times 100\ \mu m^3)$ rearrangement by agitation and an example of 100% assembly. Dark squares are hydrophilic sites and gold regions are hydrophobic surfaces.

Figure 2. Behavior of meniscus convexity at various substrate tilting angles.

(a) approach   (b) flat surface   (c) assembly
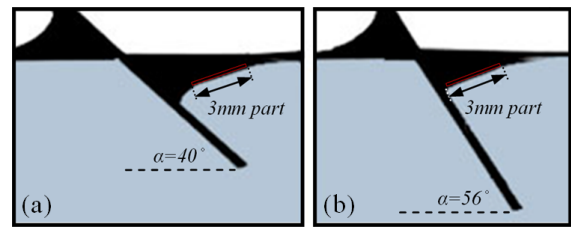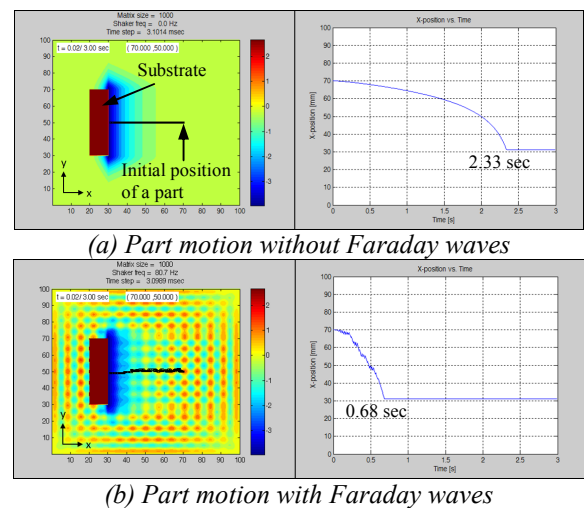Figure 3. For successful assembly, the parts go through three steps; approach, flat surface and assembly.

(a) Part motion without Faraday waves

(b) Part motion with Faraday waves
Figure 6. Simulated motion of a part $(1000 \times 1000 \times 100\ \mu m^3)$ at air-water interface. The initial position of a part is (70, 50) mm and vertical agitation with 80 Hz / 1.4 g is applied. Color indicates the surface level.

365

ASSEMBLY MODEL

The capillary torque between parts and binding site is critical to successful assembly. For the part on the binding site, if the capillary torque during transition from Figure 3(b) to (c) is not large enough to overcome the gravitational force due to an upward bending meniscus near the substrate, the part will be repelled away, which results in assembly failure.

To calculate the capillary torque between the part and site, the geometry including the part at the air-water interface and binding site is depicted in Figure 7.
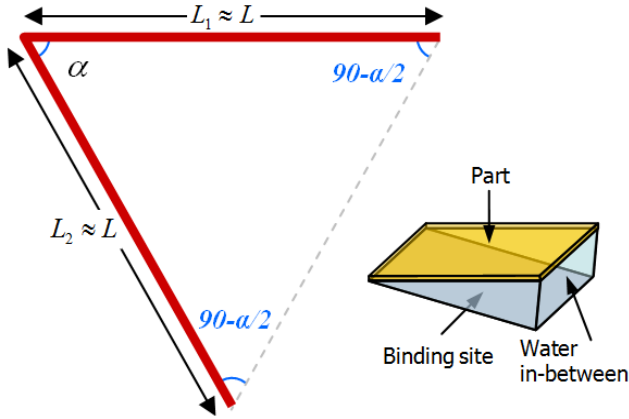

Figure 7. Simplified diagram for capillary torque model. Horizontal and inclined solid lines indicate the bottom oxide side of the part floating at the air-water interface and the oxide binding site under the water, respectively.

The ratio of body forces to surface tension forces can be expressed using the dimensionless bond number $Bo = \rho g L_c^2 / \gamma$ with ρ being the density of water, g the acceleration which is gravity, L_c the characteristic length scale and γ the surface tension of the water. The bond numbers for successful assembly are less than 1, thus the surface tension dominates during the transition from Figure 3(b) to (c) and the gravitational force is neglected.

The system has three phases (S: solid, L: liquid, V: vapor) and three interfaces (SL: solid-liquid, SV: solid-vapor, LV: liquid-vapor) which result in the total energy W_{TOT}. For equations (2)-(6), surface tensions for both part and binding sites are the same ($\gamma_{SL1}=\gamma_{SL2}=\gamma$) and part size and binding site size are $L_1 \times L_1$ and $L_2 \times L_2$, respectively, where $L_1 \approx L_2 \approx L$. The energy between oxide and air, W_{SV} can be ignored because oxide area is covered by liquid.

$$W_{SL} = \gamma_{SL1}L_1^2 + \gamma_{SL2}L_2^2 \approx 2\gamma_{SL}L^2 \qquad (2)$$

$$W_{SV} \approx 0 \qquad (3)$$

$$W_{LV} = 2\gamma_{LV}\frac{1}{2}L_1L_2 \sin\alpha \approx \gamma_{LV}L^2 \sin\alpha \qquad (4)$$

$$W_{TOT} = W_{SL} + W_{SV} + W_{LV} \approx 2\gamma_{SL}L^2 + \gamma_{LV}L^2 \sin\alpha \qquad (5)$$

Therefore, the torque T acting on the part can be expressed as a function of substrate tilting angle α after differentiating W_{TOT} with respect to α.

$$T = -\frac{dW_{TOT}}{d\alpha} = -\gamma_{SL}L^2 \cos\alpha \qquad (6)$$

Based on this model, part size scaling is analyzed in single angle assembly and feedback assembly, which uses substrate tilting angle modification to increase capillary torque after forming line contact to overcome the size limit of single angle assembly.

Single Angle Assembly

Due to decrease of the torque per unit area with increase of part size as shown in Table 1, large parts are repelled and result in no assembly. Through an additional experiment and equation (6) with 1×1 mm^2 parts for different substrate tilting angles α, we determine the critical torque per unit area for successful assembly. In this experiment, 1×1 mm^2 parts are assembled at various substrate tilting angles α up to 24.1º, which indicates the minimum torque per unit area is 0.071 μN/m. Compared with this value, 3×3 and 5×5 mm^2 parts have 0.048 and 0.022 μN/m respectively. These smaller torques per unit area cause them to be repelled by the upward meniscus during pull-up and prevent them from assembly although the parts approach the substrate and make line contact at a certain angle of $\alpha = \alpha_1$. Based on this analysis and Figure 8, the maximum part for assembly is predicted to be around 2×2 mm^2 at $\alpha = \alpha_1 \approx 25º$.

However, 3×3 and 5×5 mm^2 parts can be assembled using feedback assembly using two different substrate tilting angles. This method is discussed in the next section.

Feedback Assembly

The maximum assemblable part using single angle assembly is around 2×2 mm^2. However, we can change the substrate tilting angle α to increase the capillary torque keeping initial line contact. Once the part makes line contact at $\alpha = \alpha_1$, it tends to be pinned due to the capillary force in the contact region. This pinning effect enables changing α to a different value, $\alpha = \alpha_2 < \alpha_1$ maintaining line contact (Figure 9).

As shown in Table 1, once 3×3 mm^2 parts approach the substrate at $\alpha_1 = 48.2º$ and form line contact, the substrate is tilted down to $\alpha_2 = 19.2º$ maintaining the line contact. Thus the capillary torque per unit area reaches the critical value at $\alpha = \alpha_2$ and successful assembly is achieved. Through the same procedure, the minimum substrate tilting angles α_2 for different part sizes are experimentally determined and corresponding capillary torques are calculated based on the developed model (Table 1). Parts with different dimensions have the same capillary torques per unit area when they can be assembled.

Table 1. Single angle and feedback assembly test results. The surface tension induced torque per unit area is calculated based on the developed model. The surface tension induced torque per unit area should be larger than its critical value (0.066 µN/m) for assembly.

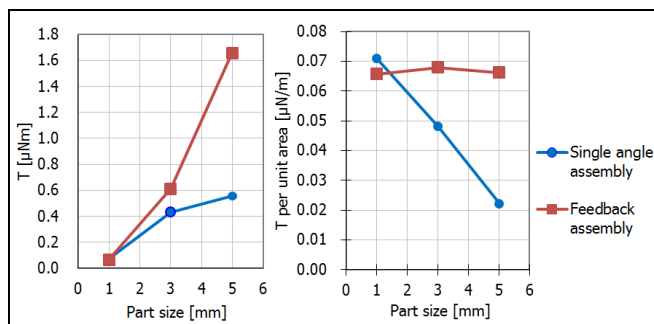| Part size $L \times L$ [mm²]	Part Volume [mm³]	Single angle assembly				Feedback assembly			
		Minimum $\alpha(=\alpha_1)$ [°]	Torque, T at α_1 [µNm]	T per unit area [µN/m]	Assembly	α_2 [°]	Torque, T at α_2 [µNm]	T per unit area [µN/m]	Assembly
1×1	0.1	< 10	> 0.07	> 0.071	Yes	24.1	0.07	0.066	Yes
3×3	0.9	48.2	0.43	0.048	No	19.2	0.61	0.068	Yes
5×5	2.5	72.1	0.72	0.022	No	23	1.66	0.066	Yes

Figure 8. Analysis of the capillary torque vs. part size (1×1, 3×3 and 5×5 mm² parts with 100 µm thickness) in single angle and feedback assembly (see Table 1).
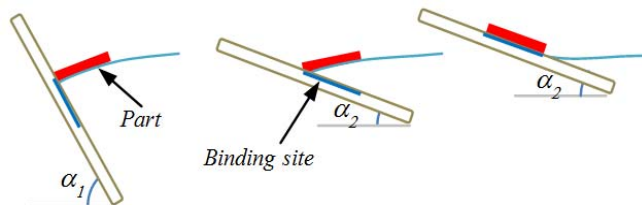

Figure 9. Schematic of feedback assembly. A part forms line contact at α_1. The critical capillary torque is obtained at α_2 and the part is assembled by pulling up the substrate.

CONCLUSIONS

The mechanics of a novel high yield fluidic self-assembly method using air-water interface is experimentally analyzed using a capillary torque model and verified using 1×1, 3×3 and 5×5 mm² parts of 100 µm thickness. The minimum torque per unit area is experimentally determined for various part sizes. In addition, a method to assemble large parts using substrate tilting angle modification is proposed and demonstrated.

REFERENCES

[1] S. A. Stauth and B. A. Parviz, "Self-assembled single-crystal silicon circuits on plastic," *Proceedings of the National Academy of Sciences of America,* vol. 103, pp. 13922-13927, 2006.

[2] H. O. Jacobs, A. R. Tao, A. Schwartz, D. H. Gracias, and G. M. Whitesides, "Fabrication of a cylindrical display by patterned assembly," *Science,* vol. 296, pp. 323-325, 12 APRIL 2002 2002.

[3] W. Zheng, P. Buhlmann, and H. O. Jacobs, "Sequential shape-and-solder-directed self- assembly of functional microsystems," *Proceedings of the National Academy of Sciences of America,* vol. 101, pp. 12814–12817, 2004.

[4] W. Zheng, J. Chung, and H. O. Jacobs, "Fluidic heterogeneous microsystems assembly and packaging," *Journal of Microelectromechanical Systems,* vol. 15, pp. 864–870, 2006.

[5] J. Tien, A. Terfort, and G. M. Whitesides, "Microfabrication through electrostatic self- assembly," *Langmuir,* vol. 13, pp. 5349-5355, 1997.

[6] S. B. Shetye, I. Eskinazi, and D. P. Arnold, "Self-assembly of millimeter-scale components using integrated micromagnets," *IEEE Transactions on Magnetics,* vol. 44, pp. 4293-4296, 2008.

[7] H. Ye, Z. Gu, T. Yu, and D. H. Gracias, "Integrating nanowires with substrates using directed assembly and nanoscale soldering," *IEEE Transactions on Nanotechnology* vol. 5, pp. 62–66, 2006.

[8] R. J. Knuesel and H. O. Jacobs, "Self-assembly of microscopic chiplets at a liquid-liquid-solid interface forming a flexible segmented monocrystalline solar cell," *Proceedings of the National Academy of Sciences of America,* vol. 107, pp. 993-998, 2010.

[9] M. Boncheva, D. A. Bruzewicz, and G. M. Whitesides, "Millimeter-scale self-assembly and its applications," *Pure and Applied Chemistry,* vol. 75, pp. 621-630, 2003.

[10] T. B. Benjamin and F. Ursell, "The Stability of the Plane Free Surface of a Liquid in Vertical Periodic Motion," *Proceedings of the Royal Society of London. Series A, Mathematical and Physical Sciences,* vol. 225, pp. 505-515, 1954.

[11] S. Douady and S. Fauve, "Pattern Selection in Faraday Instability," *Europhysics Letters,* vol. 6, pp. 221-226, 1988.